Mechanism of Silver(I)-Assisted Growth of Gold Nanorods and Bipyramids

Mingzhao Liu and Philippe Guyot-Sionnest*

James Frank Institute, The University of Chicago, 5640 South Ellis Avenue, Chicago, Illinois 60637

Received: August 25, 2005; In Final Form: September 16, 2005

The seed-mediated growth of gold nanostructures is shown to be strongly dependent on the gold seed nanocrystal structure. The gold seed solutions can be prepared such that the seeds are either single crystalline or multiply twinned. With added silver(I) in the cetyltrimethylammonium bromide (CTAB) aqueous growth solutions, the two types of seeds yield either nanorods or elongated bipyramidal nanoparticles, in good yields. The gold nanorods are single crystalline, with a structure similar to those synthesized electrochemically (Yu, Y. Y. et al. *J. Phys. Chem. B* **1997**, *101*, 6661). In contrast, the gold bipyramids are pentatwinned. These bipyramids are strikingly monodisperse in shape. This leads to the sharpest ensemble longitudinal plasmon resonance reported so far for metal colloid solutions, with an inhomogeneous width as narrow as 0.13 eV for a resonance at ∼1.5 eV. Ag(I) plays an essential role in the growth mechanism. Ag(I) slows down the growth of the gold nanostructures. Ag(I) also leads to high-energy side facets that are {110} for the single crystalline gold nanorods and unusually highly stepped {11*n*} ($n \sim 7$) for the bipyramid. To rationalize these observations, it is proposed that it is the underpotential deposition of Ag(I) that leads to the dominance of the facets with the more open surface structures. This forms the basis for the one-dimensional growth mechanism of single crystal nanorods, while it affects the shape of the nanostructures growing along a single twinning axis.

Introduction

Noble metal nanocrystals have interesting optical properties that come from the excitation of free electron plasmon by the electromagnetic field.[1,2] These plasmon modes give rise to strong light absorption and scattering. The plasmon modes of a metal particle are determined by its shape, composition, size, and surrounding media.[2] Although spherical nanoparticles can be synthesized easily, the tunability of the plasmon is small since its frequency is independent of the size as long as $R \ll \lambda$. Instead, the resonance frequency is very sensitive to the shape of the nanoparticles. In recent years, metal nanoparticles with different shapes have been synthesized, with their spectra covering the whole visible and near-infrared range (∼0.6−3 eV). The shapes explored include prisms,[3,4] spherical shells,[5] cubes,[6] rods,[7−10] and wires.[11]

The rodlike nanoparticles are promising systems for optical studies as the spectrum is easily tunable by varying the aspect ratio. For example, we reported on gold nanorods, where the longitudinal plasmon resonance is tunable from 2.4 to 0.6 eV by increasing the aspect ratio from 1 (sphere) to 13.[12] Compared to spheres, the quasi-one-dimensional structure gives a larger curvature at the tips for the same volume. Since the local field enhancement is proportional to the curvature of the surface,[13] significant field enhancement is also expected for the nanorods. Furthermore, the closer coupling achievable with rods is beneficial for energy transfer processes.

During the past decade, several methods have been developed to synthesize gold nanorods. Gold nanorods were synthesized by Van der Zande et al., using porous alumina as a hard template.[14] However, this method only yields very small amounts of nanorods for each synthesis.

The electrochemical reduction method developed by Yu et al. provided higher yields.[7] This method consists of electrochemically reducing $HAuCl_4$ in an aqueous solution of CTAB (cetyltrimethylammonium bromide), a cationic surfactant, and it yields gold nanorods with an aspect ratio of 2−7 and decent selectivity. These nanorods were shown to be single crystalline by high-resolution transmission electron microscopy (HRTEM) studies.[15,16] The nanorods were grown along the [100] direction, with the side walls as the {110} and {100} facets. The growth mechanism, together with the stabilization of the more open {110} facets, remained unclear.

Inspired by the idea that CTAB may act as a soft template, the seed-mediated method was developed by Murphy and co-workers. In this method, nanorods are produced in reasonable yield by chemically reducing $HAuCl_4$ in a CTAB solution, with small seed gold nanoparticles added as nucleation centers.[8] Using selective area electron diffraction (SAED) and HRTEM, Johnson et al. showed that the nanorods are isometric pentafold twinned around their growth axis, which is along the [011] direction.[17] Each section is separated by (111) planes. In an idealized model, each nanorod has five {100} side faces and ten {111} end faces. The elongation along the twinning axis was naturally explained by the different growth rates of the {100} facets and {111} facets. As an alternative explanation, Mulvaney and co-workers proposed that the tip of nanorods experiences a stronger static electric field, such that more gold ions can be driven and deposited to the tip.[18] However, this theory does not simply explain the initial change of morphology from the seed, which is almost spherical.

In the prior electrochemical synthesis, it had been noticed that the aspect ratio of the nanorods could be controlled by introducing silver ions into the solution.[19] Building up on the idea of using gold seeds as nucleation centers but adding Ag(I) of varying concentrations in the growth solution, El-Sayed and co-workers developed an alternative procedure to produce gold

* Corresponding author. Phone: (773) 702-7461; fax: (773) 702-5863; e-mail: pgs@uchicago.edu.

10.1021/jp054808n CCC: $30.25
Published on Web 10/22/2005

nanorods in even higher yield, with the aspect ratio easily controlled by the silver concentration.[10] However, the role of silver was not simple since when adding Ag^+ into the procedure used by Murphy and co-workers nanorods are no longer formed, but instead, some so-called ϕ-shaped nanoparticles were formed.[20,21]

Therefore, although both seed-mediated growth procedures yield gold nanorods, they are not interchangeable and seem to operate via rather different routes. A couple reports did briefly mention that the nanorods grown in the presence of silver may be single crystalline and similar to those grown electrochemically.[10,22] This is in striking contrast to the pentatwinned nanorods grown without silver. This is an important clue of one major difference between the two products, but it has not been pursued further, and there have been no detailed structural characterizations. To date, there is also no satisfactory description of the critical role played by the silver ions. Furthermore, while the seed-mediated approach is so successful and the role of the size and surface charge has been studied by Murphy et al.,[23] little attention has been given to the possibly important role of the seed structure, even though it is well-known that the structure of the small metal nanoparticles can be complex and not necessarily single crystalline.[3,24,25]

In this paper, we characterize the structures of the gold seeds and reveal that two basic types of gold seeds are obtained in different preparations. One is single crystalline and another is multiply twinned. We demonstrate the importance of the seed structure by showing that the silver assisted growth products from these two types of gold seeds are completely different, producing either single crystalline nanorods or penta-fold twinned bipyramid-shaped nanoparticles, respectively. Furthermore, both final structures have higher energy surface structures, which are not commonly seen for the growth without silver. We then propose a mechanism whereby Ag(I) has an earlier underpotential deposition onset on these higher energy surface structures. Ag(0) therefore acts as a surfactant slowing down the growth rate of these faces, which become dominant.

Experimental Procedures

CTAB and L-ascorbic acid were purchased from Fluka. A standard 1 M HCl solution was purchased from Fisher. All other chemicals used in the experiments were purchased from Sigma-Aldrich without further purification. The HRTEM images of the samples were acquired with an FEI Tecnai F30 microscope operating at 300 kV.

Preparation of Gold Seeds. Small gold nanoparticles were prepared as the seeds for the growth of gold nanostructures by reducing $HAuCl_4$ with $NaBH_4$ or L-ascorbic acid.

The first type (Type *I*) was prepared following the method developed by Nikoobakht and El-Sayed.[10] A total of 0.25 mL of 10 mM $HAuCl_4$ was mixed with 10 mL of a 0.1 M CTAB solution at 30 °C. Next, 0.60 mL of a freshly prepared 10 mM $NaBH_4$ solution was injected quickly into the solution under vigorous stirring. The gold sol was stirred for at least 5 min for the complete decomposition of excess $NaBH_4$.

The second type (Type *II*) was prepared via the procedure of Jana et al.[8] To a 20 mL solution containing 0.125 mM $HAuCl_4$ and 0.25 mM sodium citrate under vigorous stirring, 0.3 mL of 10 mM freshly prepared $NaBH_4$ solution was added at room temperature. The gold sol was aged at room temperature for at least 2 h before use. UV−vis spectra showed that the characteristic plasmon resonance of gold nanoparticles at 520 nm was damped to various degrees for these two types of gold seeds, indicating that the particles were smaller than 5 nm.

Silver(I)-Assisted Growth of Gold Nanorods. The original method developed by El-Sayed and co-workers gives nearly quantitative yield of gold nanorods.[10,22] However, it was observed by us and others that the freshly prepared nanorods can further grow into a dumbbell shape, causing the longitudinal plasmon resonance to blue-shift by up to 100 nm over the first few hours.[22,26] We found that controlling the pH allowed us to significantly improve the method and product stability. In a typical synthesis, 0.5 mL of 10 mM $HAuCl_4$ and 0.1 mL of 10 mM $AgNO_3$ were mixed with 10 mL of a 0.1 M CTAB solution. The solution was then acidified with 0.2 mL of 1.0 M HCl to pH 3∼4, followed by the addition of 0.08 mL of 0.1 M L-ascorbic acid, which reduced Au(III) to Au(I). Finally, 24 μL of gold seeds *I* was injected into the growth solution. The growth reaction was performed at 30 °C under gentle stirring. The reduction ended within 2 h. The effect of $AgNO_3$ was studied by varying its amount from 0 to 0.1 mL. For the growth from gold seeds *II*, more seed solution (80 μL) was used because of their larger particle size and therefore lower particle concentration.

Results and Discussion

Structures of the Gold Seeds. Although the spectra of seeds *I* and *II* showed that their diameters were smaller than 5 nm, they were seen to be much larger in the initial TEM images. This is likely because these ultra-small particles experience Ostwald ripening on the TEM grid, as the solution was dried. To acquire the real images of these nanoparticles, long chain thiols (*n*-dodecanethiol) were used to cap the nanocrystal seeds at room temperature so that they would not grow further. The gold seeds *I* were still soluble in the CTAB solution after the treatment. However, the thiol-capped gold seeds *II* could not be charge-stabilized by citrate anymore and were extracted into chloroform.

TEM images of these thiol-capped nanoparticles are shown in Figure 1. The diameters of the seeds *I* are around 1.5 nm, with a standard derivation of order 10%. The important feature is that the majority of the particles appear single crystalline in the high-resolution TEM. As shown in the histogram in Figure 1a, when the lattice fringes are clearly visible, it is very rare to observe a twin structure.

The diameters of the seeds *II* are larger, around 3 nm, and rather monodisperse. In stark contrast to seeds *I*, the TEM shows that most of the nanoparticles for which lattice fringes are clearly seen are twinned crystals. We note that this is in contrast to a previous report.[17] The twinned crystals, if oriented properly, can be seen to have pentagonal symmetry (Figure 1b). This kind of structure has been commonly seen for small noble metal clusters, and it is generally recognized as a decahedron where the twinned crystal has five twin boundaries, which are all (111) planes.[3,24,25] This configuration determines the twinning axis to be [011].

Growth from Gold Seed I. As indicated by the UV−vis spectra in Figure 2, the gold seeds *I* are grown into nanorods in high yield (≥95% from TEM images) with the assistance of Ag(I). By increasing the concentration of Ag(I) from 0.1 to 0.5 mM, the longitudinal plasmon resonance red-shifts from 2 to 1.4 eV, corresponding to an increase of the aspect ratio from 2 to 5, as confirmed by the TEM. We note that the gold nanorods grown to such different aspect ratios nevertheless preserve an approximately similar volume, which is consistent with the gold seeds nucleating the growth. Importantly, the high-resolution TEM images in Figure 3 show that the nanorods are single crystals with no observable stacking faults or twins. This is

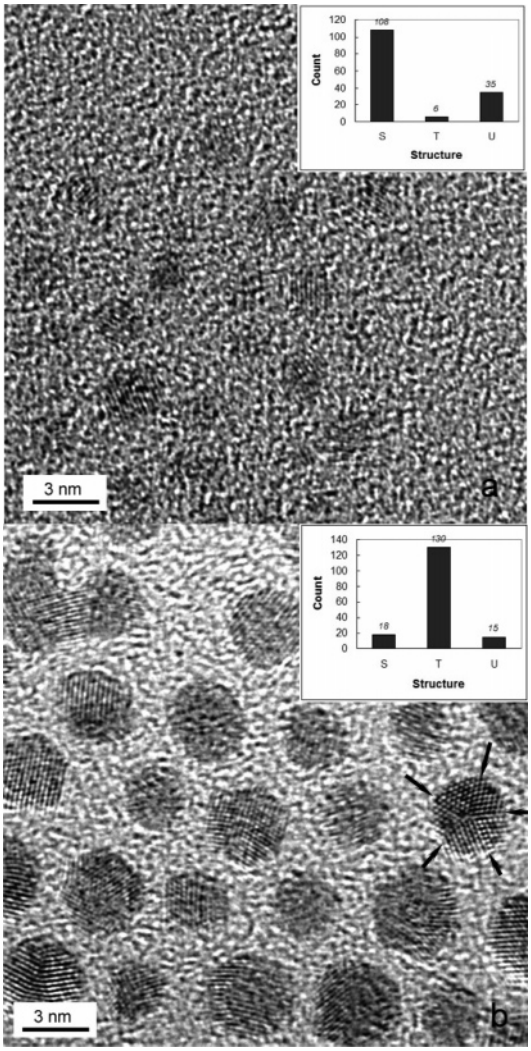

Figure 1. (a) High-Resolution TEM image of gold seeds *I*. (b) High-resolution TEM image of gold seeds *II*. One of the seeds shows a very clear penta-fold twinning. The twinning planes are indicated by the arrows. The histograms are plotted by counting about 150 nanoparticles from different areas on the TEM grid for each sample. S, T, and U stand for single crystalline, twinned, and unidentified nanoparticles, respectively. There are more unidentified particles for type *I* because of their smaller size and therefore worse contrast.

independent of the silver concentration in the range studied. The nanorods grow in the [100] direction (i.e., by the stacking of (100) planes along the axis). For a fresh sample, the ends of the nanocrystals are nearly flat, which must be the {100} facets. The aged samples generally develop more truncated ends.

TEM images cannot tell the shape of the cross-section of the nanorods directly. However, since the excess surfactant has been removed by its crystallization from cold solution (~5 °C), most nanorods should lay on the carbon film with one side surface parallel to it (i.e., normal to the electron beam). For a fully grown nanorod sample, both [011] and [001] orientations were seen. Therefore, the sidewalls of the nanorods should be {110} and {100} facets. This structure is identical to the gold nanorods synthesized electrochemically.[7,15,16] Since the electrochemically synthesis of gold nanorods is also assisted by Ag(I),[19] silver should play the same role for both cases. However, the structure is totally different from the seed-mediated grown gold nanorods in the absence of Ag(I),[17] suggesting a different growth mechanism.

We made the observation that the growth reaction can be terminated at anytime, by adding *n*-dodecanethiol to the solution,

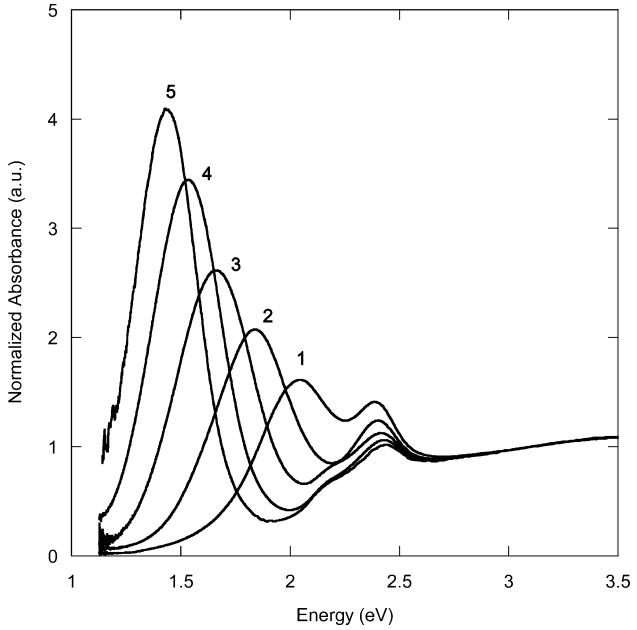

Figure 2. UV−vis spectra of gold nanorods grown from gold seed *I*. The concentrations of Ag(I) are 0.1, 0.2, 0.3, 0.4, and 0.5 mM for samples 1−5, respectively. Each spectrum is normalized by its absorption at 3.1 eV (400 nm).

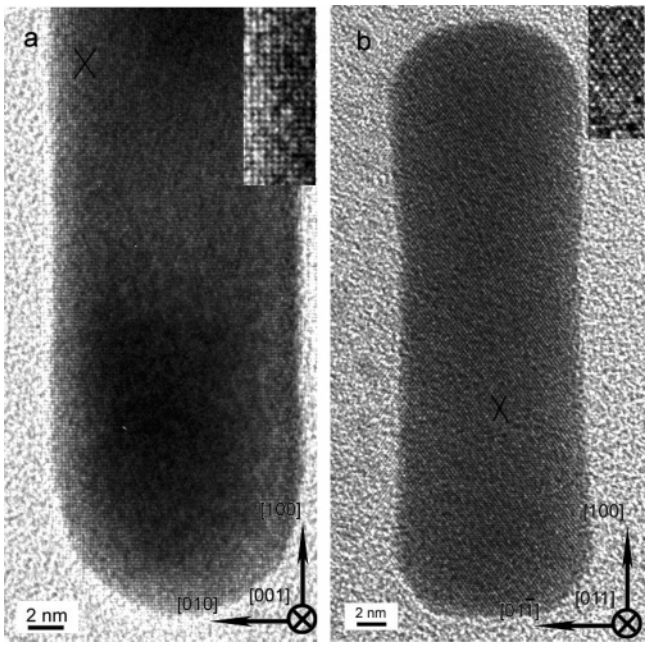

Figure 3. High-resolution TEM images of gold nanorods grown from gold seeds *I* with silver (I). The nanorods are aligned in [001] (a) and [011] (b) directions. The insets show 2× magnifications of the areas labeled by the black crosses. The dimensions of the insets are 2 nm × 5 nm for panel a and 2 nm × 4.6 nm for panel b.

leaving the smaller, unfinished nanorods capped by thiol. Most of these nanorods have a [011] orientation on the carbon grid, instead of [001], indicating that the {110} facets are in fact dominant during the growth process. Therefore, the {100} facets observed for the fully grown nanorods are more likely to have appeared during the aging. This thiol-quenching experiment also gives information on how the shape of the nanorods evolves during the growth. The growing particles are indeed found to be rod-shaped as early as their volume is about 5% of the final volume, and the aspect ratio changes little after their volume is about 10% of the final volume. This indicates that the growth-

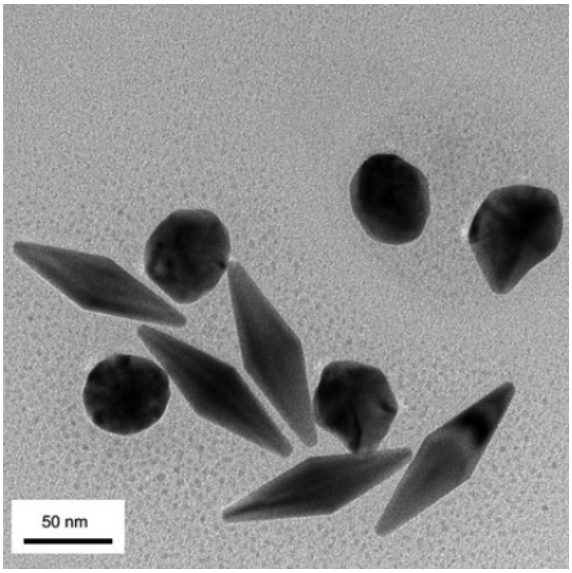

Figure 4. TEM image of gold nanostructures grown from gold seeds *II* with silver(I).

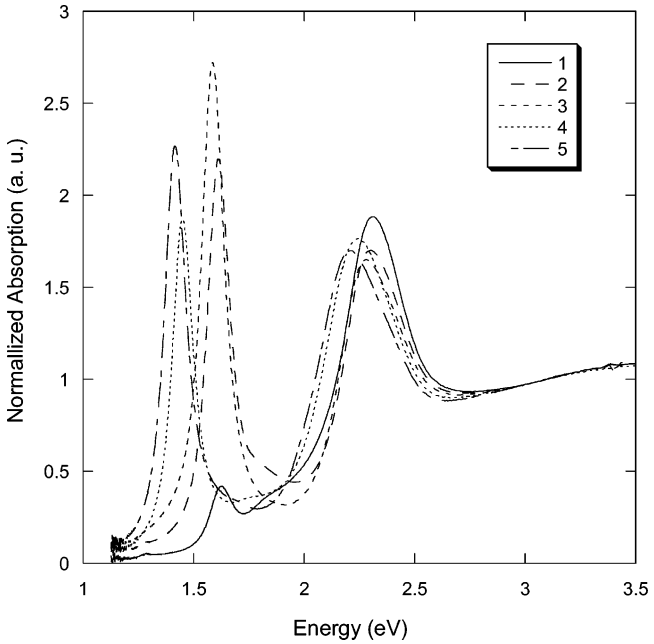

Figure 5. UV−vis spectra of different gold nanobipyramid solutions. No size or shape selection was performed. For samples 1−3, the gold seeds used were aged at room temperature (~22 °C) for 24 h. The Ag(I) concentrations are 0.1, 0.2, and 0.4 mM, respectively. For samples 4 and 5, the gold seeds used were aged at 5 °C for 24 h. The Ag(I) concentrations are 0.2 and 0.4 mM, respectively. The other conditions are the same. Each spectrum is normalized by its absorption at 3.1 eV (400 nm). Higher Ag(I) concentrations lead to higher yield of the bipyramids, up to about 30% as seen by TEM. The narrow peak at ~1.5 eV is the longitudinal plasmon of the bipyramids. The absorption around 2.3 eV corresponds to the transverse mode of the bipyramids and the other nearly spherical nanoparticles.

rate ratio between the (110) surface and the (100) surface is constant for a given Ag(I) concentration. The differentiation of the side and end facets first reported here, with slowly growing (110) sides and faster growing (100) ends, provides a natural explanation for the monodisperse rod shape once an initial random symmetry breaking event has occurred.

Growth from Gold Seed II. When using the gold seeds *II*, a novel gold nanostructure with bipyramid-shape is synthesized with well-defined facets, as shown in Figure 4. An apparently

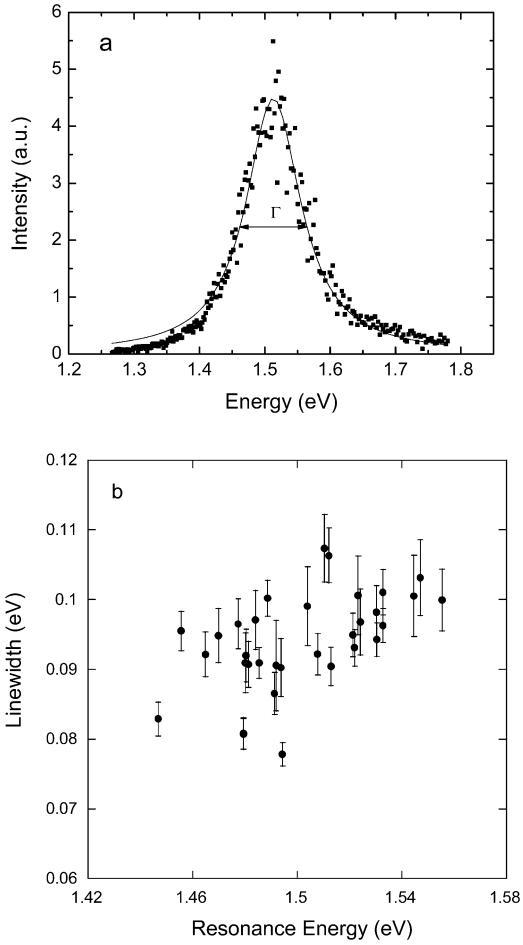

Figure 6. (a) Light scattering spectrum from a single gold bipyramid. The dots are the experimental data, and the curve is a Lorentzian fit. (b) Measured line width Γ of light scattering spectra of single gold bipyramids vs their resonance energy.

similar structure was reported by Jana et al., under the name spheroid or ϕ-shaped particle.[20,21] This structure was then regarded as the byproduct of the synthesis of nanorods, and it had not been the subject of detailed structural or optical characterization.

We noticed, however, that the bipyramids have a strikingly pronounced near-IR absorption peak around 1.5 eV (Figure 5), which corresponds to the longitudinal surface plasmon mode. Such a sharp absorption feature is unheard of in metal colloid solutions, and it deserves further discussion. The yield of the bipyramids is estimated to be about 30%.

For nanorod solutions with a similar plasmon resonance, the inhomogeneous line width is at least 0.3 eV as shown in Figure 2. For the bipyramid solutions, the inhomogeneous line width of the longitudinal plasmon resonance is much smaller, as small as 0.13 eV.

The homogeneous line width of the longitudinal plasmon resonance of the bipyramids was studied by measuring the white light scattering spectra from single bipyramids. The aqueous colloids are transferred to a methanol solution with 1% PVP (poly(vinylpyrrolidone)) and drop-cast onto clean glass slides. The sample is investigated using a 40× objective and is illuminated by a halogen lamp through a high aperture dark-field condenser.[27] For spectral analysis, the scattered light from each nanoparticle is focused onto the entrance slit of a grating spectrometer and detected by a nitrogen-cooled CCD camera. A typical scattering spectrum from a bipyramid is shown in Figure 6a, with a quasi-Lorentzian line shape. In Figure 6b, the

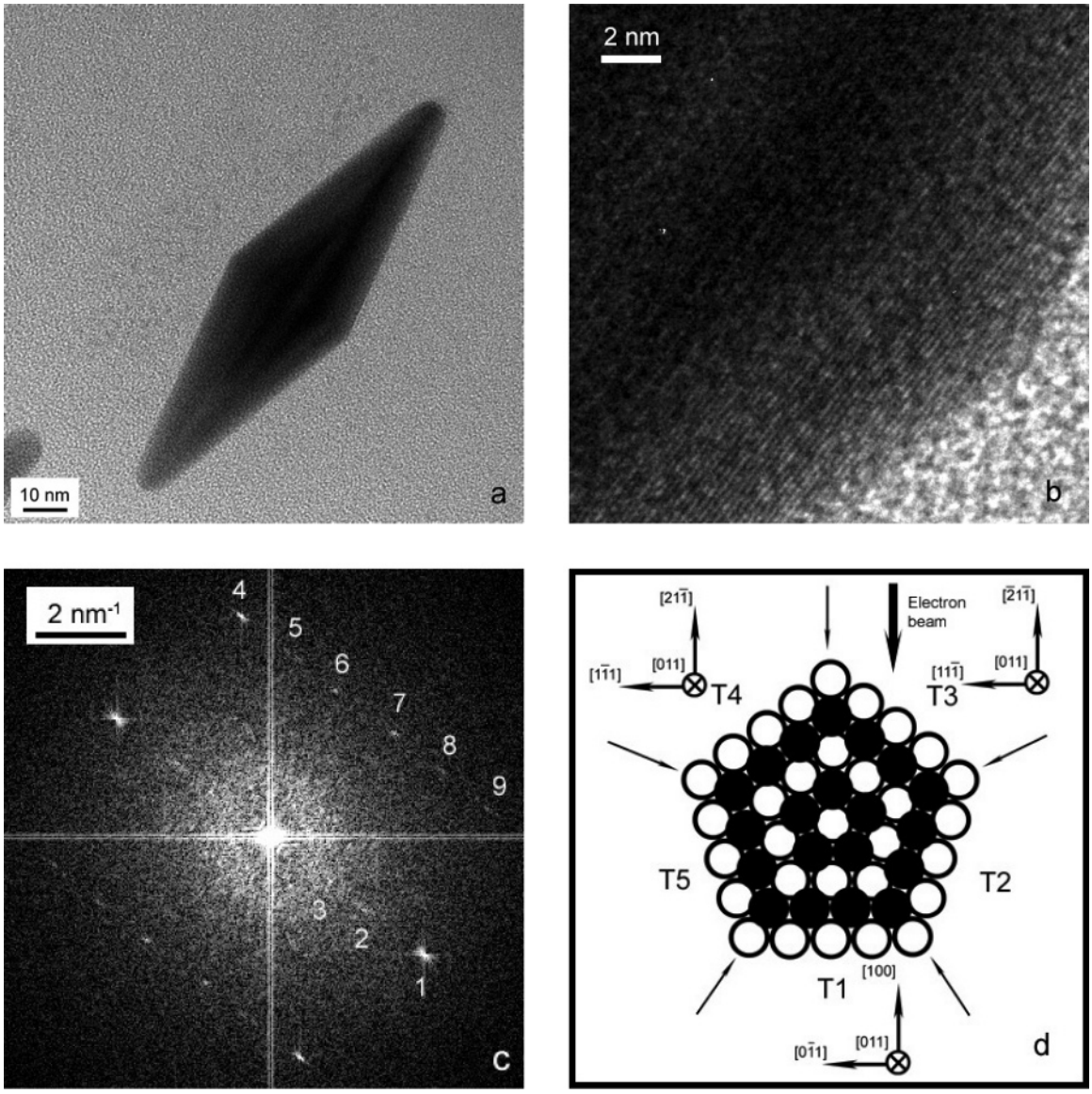

Figure 7. (a) High-resolution TEM image of a nanobipyramid and (b) the magnification of its equatorial part. (c) The power spectrum of the image. (d) The cross-section perpendicular to the growth axis of the penta-fold twinned structure. Each section was labeled as T1, T2, T3, T4, and T5, respectively, with the twinning planes pointed by the arrows. The close circles stand for gold atoms on the cross-section layer. The open circles stand for the layer below.

line widths are plotted against the resonance energy for 33 bipyramids. The line widths are 94 ± 7 meV, and the resonance energies are 1.50 ± 0.03 eV. The line widths are broader than those of gold nanorods (~80 meV).[12,27] The extra line width is attributed to a contribution from the radiative plasmon decay because the bipyramids have a larger volume than the nanorods and therefore a larger radiative decay rate.

The narrow inhomogeneous line width suggests that the bipyramids have a very small variance on their shape. Indeed, the TEM images show that the variance of the tip angles is as small as $\pm 1°$ within each sample. For different samples, the average tip angle varies only from 26 to 30°. The longitudinal plasmon resonance, present in the range of 1.4−1.6 eV, not only depends on the tip angle but also on the tip truncation. Both factors appear to be quite sensitive to the quality of the gold seeds *II*, which itself depends on the reduction temperature and aging conditions. In comparison to the determinant role of the seeds in producing the bipyramids, the effect of the Ag(I) concentration is rather small, although Ag(I) is needed to form this structure.

TEM images show that there is a diffraction contrast along the growth axis of each bipyramid, indicating that the structure is not single crystalline. The structure is twinned along the long axis. A high-resolution image is shown in Figure 7, showing clear fringes parallel to the growth axis along both sides. The spacing is given as 0.232 nm by a direct measurement, by which the fringes are indexed as (111) planes. Similar fringes in the central region are shown as wider stripes, with more structures. These fringes are difficult to index by a direct measurement, and they have to be measured from the power spectrum (i.e., the modulus of the Fourier transform of the image). The power spectrum in Figure 7c shows three pairs of diffraction patterns labeled as 1, 2, and 3, which are aligned in a line across the center and normal to the long axis of the bipyramid. Six pairs of sideband reflections are also shown and labeled as 4−9. They correspond to the following lattice parameters: $d_1 = 0.232$ nm, $d_2 = 0.376$ nm, $d_3 = 0.613$ nm, $d_4 = d_9 = 0.201$ nm, $d_5 = d_8 = 0.241$ nm, and $d_6 = d_7 = 0.276$ nm. This pattern is almost identical to a simulated result reported by Lisiecki et al., which is based on a cyclic penta-twinned copper nanocrystal.[28,29] This

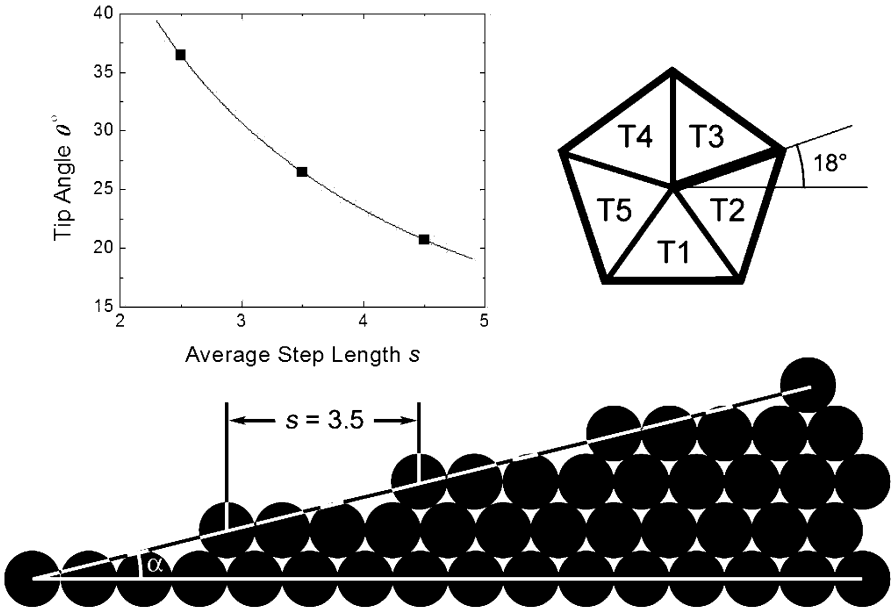

Figure 8. Bottom schematic illustrates the interface between T2 and T3 of a gold bipyramid, which is oriented as shown in the right inset and has a 3.5 atom step length. For this orientation, which is most commonly seen in the TEM images, the measured tip angle θ is a function of α in the form $\theta = 2 \arctan(\tan \alpha \cos 18°)$. The angle α is related to the average step length s by the equation $\tan \alpha = \sqrt{3}/2s$. The left inset shows the relation between the tip angle and the average step length. The experimental value of θ is 26−30°, corresponding to the average step length of ~3.5.

suggests that the bipyramid should have the same penta-fold twinning structure, although its shape requires different facets. This twinning structure is also seen for some of the gold seed *II* as well as the gold nanorods synthesized by Murphy and co-workers.[17]

An illustration of the equatorial cross-section of this possible structure is shown in Figure 7d. On this basis, the experimental power spectrum pattern can be indexed as following. Diffraction 1 resembles the reflections from the $(11\bar{1})$ of T3 and the $(1\bar{1}1)$ of T4. Diffractions 4 and 9 are the (002) and (020) reflections, respectively, from T1. The angle between diffraction 4 and the growth axis is 45°, and it is the same as for diffraction 9. The measured values agree with the bulk data within 2%, which are 0.235 and 0.204 nm, for (111) and (002), respectively. Diffractions 2, 3, and 5−8 should be multiple scatterings effects. For example, one notices that $d_2 = d_{(111)} + d_{(220)}$. However, no reflection from the (220) type surfaces is seen since it is forbidden in a bulk fcc structure.[28] Another evidence for the penta-fold cross-section is the clear (111) fringes on both sides because the electrons that pass through those areas are only diffracted by T3 or T4, without T1 involved.

The gold nanorods reported by Johnson et al. have exactly the same twinning structure and equatorial cross-section as the gold bipyramids.[17] This similarity gives them similar surfaces, which are {100} facets. For the nanorods, each {100} facet is flat along the growth direction.

For the bipyramids, the {100} facet has to be stepped periodically along the growth direction to fit the geometry. An idealized cross-section along the growth axis is shown in Figure 8, indicating that the average step length should be ~3.5 atoms to give the tip angle beween 26 to 30°. Thus, the stepped facet is indexed as ~(117).

We propose that the unique geometry of these bipyramids could be interesting for the study of plasmonics. They have similar or larger dimensions than the nanorods, with the length about 80 nm and the equator diameter about 20 nm, but they have a much sharper apex. The sharp apex should provide larger near-field enhancement at the plasmon resonance. Furthermore, the narrow ensemble spectrum may increase the sensitivity for sensing modification of the near-field environment, without having to resort to single particle measurements. For other photonic applications, it may be also critical to achieve highly perfect and monodisperse nanostructures. In this case, shape control based on geometric constraints such as the bipyramid reported here may be a fruitful general approach.

Growth Mechanism. From the two sets of experiments discussed previously, it is apparent that the seed structure is determinant. The gold seeds *I*, which are single crystalline, grow into single crystalline nanorods, while in the same growth solution, the gold seeds *II*, mostly multiply twinned, grow into multiply twinned structures and, in particular, into the penta-twinned bipyramids.

We therefore propose that, when assisted by Ag(I), the deposition of gold atoms over the seed surfaces creates little or no stacking default, thus preserving the initial twinned structure into the final product. This defect-free deposition is a unique property of the growth assisted by Ag(I). It was also observed that the silver(I) assisted growth is significantly slower, which is apparent by monitoring the spectrum of the growth solution. It takes about 2 h until the end of the growth, with 0.5 mM $AgNO_3$ added to the solution. In contrast, a silver-free control experiment takes less than 45 min. The slower growth rate in the presence of Ag(I) may allow the gold atoms to be deposited at the most energy favorable place (i.e., in an fcc stacking series) and create no defect at all.

As a control, if gold seeds *I* are grown a bit larger by adding $HAuCl_4$ and ascorbic acid to the solution, without silver present, the solution then contains both single crystalline and multiply twinned nanoparticles. As expected, the Ag(I)-assisted growth from this mixture yields crystalline nanorods, together with twinned bipyramids (Figure 9a). As another control, if no silver is added, and the single crystalline gold seeds *I* are used, a noticeable amount of very long, twinned nanorods (aspect ratio up to 30), is formed in the final solution (Figure 9b). Therefore, our first conclusion is that silver(I)-assisted growth gives

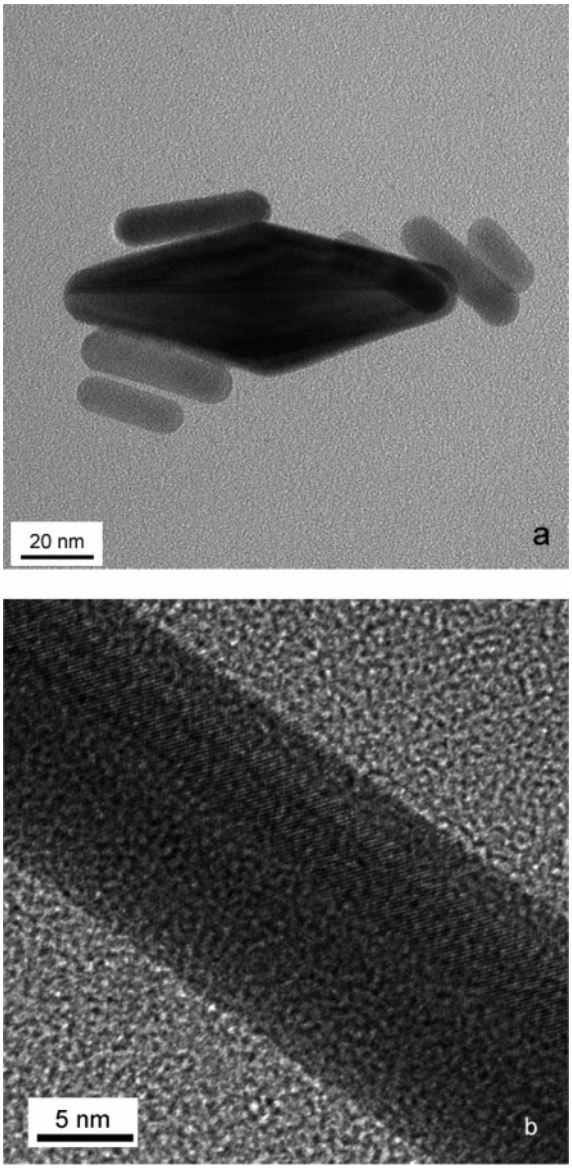

Figure 9. (a) Using gold seeds *I* that have been first grown a bit larger by adding $HAuCl_4$ and ascorbic acid to the solution, Ag(I) assisted growth then leads to a mixture of nanorods and nanobipyramids. (b) The growth from single crystalline gold seeds *I* with no Ag(I) added gives twinned nanorods.

nanostructures with a crystal structure that derives directly from the seeds with no new twin defects.

However, from an high-resolution TEM study, we can also conclude that the growth assisted by Ag(I) leads to a priori energy unfavorable surface structures. Indeed, the single crystalline nanorod has its four side surfaces as {110} facets, which rarely appear in gold nanocrystals. The {110} facet is not a densely packed surface, and it has higher energy than the {100} and {111} facets.[16] For the bipyramids, the stepped (11*n*) side facets must be of higher energy as well because the atoms on the edge of the step are very open. The area of the steps is about one-quarter of the whole surface, which is very large. In fact, we know of no other nanostructures of noble metals that exhibit such highly stepped dominant facets.

For the single crystalline gold nanorods synthesized electrochemically, it was proposed that the anisotropic growth arises from the selective adsorption of CTAB on the {110} facets. However, the essential role of Ag(I) in the seed-mediated synthesis cannot be explained from that argument. Previous reports noticed this problem and proposed that it is the silver bromide formed in solution, instead of the bromide ions, that is selectively adsorbed onto the gold surfaces.[10,22] This mechanism, although successfully including Ag(I) as a part of the argument, neglects the fact that silver bromide is not likely a more competitive adsorption agent than the bromide ion. First, the silver bromide molecule is chemically inert because of its closed-shell electronic structure and has no net charge but a permanent dipole. Second, as compared to the bromide ions in solution, the silver bromide in solution is only a small fraction ($\leq$0.5%) and mostly in a colloidal form ($k_{sp}(AgBr) = 5.35 \times 10^{-13}$). Therefore, we believe that there should be another mechanism for the anisotropic growth of single crystalline gold nanorods, including the nontrivial role of silver.

It was believed that Ag(I) in the CTAB solution can be reduced to its elemental form by ascorbic acid only in a basic pH.[30] Our previous report also confirmed that the bulk deposition of silver on the surface of gold nanorods only happens at pH $\geq$ 8 in CTAB solution, with ascorbic acid as the reducing agent.[12] For the experiments reported here, the pH of the growth solution is about 3, and the change of the reduction potential of ascorbic acid can be evaluated from the Nernst relation, yielding a reduction potential about 0.3 V higher than the one at pH 8. Therefore, silver is indeed not reducible in acidic solution.

This argument applies to the bulk deposition of Ag(0). However, a metal submonolayer or monolayer can be deposited onto a different metal surface at a potential significantly less negative than for bulk deposition. This is called underpotential deposition (UPD).[31,32] For certain systems, this underpotential shift can be as large as 0.5 V. This effect can be qualitatively accounted for by two effects. The first one is that the activity of the adlayer is smaller than the bulk value (unity), if only a submonolayer is formed. This is only significant for very low coverage. The second effect is dominant for most cases and is due to the lower chemical potential of the adsorbate as compared to its bulk value. On the basis of the theory of Kolb et al., the second term is positive only when the work function of the bulk of the adlayer metal is lower than that of the substrate.[31] The theory also showed that the underpotential shift is proportional to the work function difference, which is in qualitative agreement with experiments.[33] The work function of silver is lower than that of gold by more than 0.5 eV; therefore, the UPD of silver over gold is expected, which is actually one of the earliest UPD systems discovered.[34] Detailed electrochemical studies on single crystalline metal substrates have also shown that the UPD shifts are related to the surface structure, which can be partially understood by the fact that different surfaces have different work functions. Leiva further pointed out that it is important to consider the binding energy of the ion cores of the adsorbate, instead of solely considering the electronic part.[35] This term favors the stabilization of the adsorbate layer over a more open surface since the adatom on a more open surface has more neighbors and therefore experiences stronger attractive potential (Figure 10).

For Au and Ag, the work function differences are 0.83, 0.85, and 0.57 eV for their (100), (110), and (111) planes, respectively. Clearly, Au(111) should have much lower UPD shift for Ag^+ than the other two planes. For the comparison between (100) and (110) planes, one may further notice that (110) is a more open surface than (100). These considerations lead to the expectation that the UPD shifts of silver on gold surfaces should be in the order (110) > (100) > (111). This conclusion is in qualitative agreement with the experiment results, which give UPD shifts of 0.07 [36] and 0.24 V[37] for the formation of a

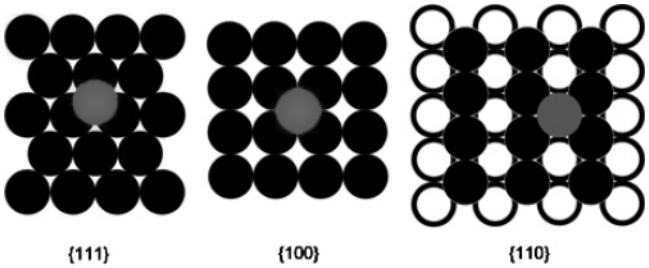

Figure 10. This schematic illustrates that an underpotential deposited silver atom (gray circles) has more nearest neighbors on a more open facet. For Au{111} facets, each silver atom has three nearest neighbors. For Au{100} facets, each silver atom has four nearest neighbors. For Au{110} facets, each silver atom has five nearest neighbors (one is in the second layer right beneath the silver atom). The gold atoms of the first layer are represented by black closed circles. For the Au{110} facets, the gold atoms of the second layer (open circles) are also partially exposed.

compact monolayer of silver over Au(111) and Au(100), respectively. However, the experimental data on Au(110) is not available. On the basis of the formation of a compact Ag monolayer, Sanchez et al. calculated the UPD shifts for the Au/Ag^+ system as 0.12, 0.17, and 0.28 V for Au(111), Au(100), and Au(110), respectively,[38,39] which is also roughly consistent with the qualitative analysis stated previously. Supporting evidence is also given by the completely studied Au/Pb^{2+} system, where the lead monolayer is formed on Au(110) at a potential at least 0.1 V more positive than Au(111) and Au(100).[40,41]

From the previous discussion, we know that the reduction potential of ascorbic acid in our system is about 0.3 V higher than for bulk deposition of silver in the growth solution. At this potential, a compact silver monolayer can be formed preferably on the {110} facets of the gold nanocrystals. It suggests that the dominance of the otherwise higher energy {110} facets on the single crystalline gold nanorods can be explained by this UPD effect. The silver monolayer over Au{110} acts as a strongly binding surfactant to protect the facet from further growth. The silver layer can be oxidized and replaced by the gold ions in the solution. However, the total growth rate of gold on {110} facets may be significantly slowed. The top of the nanorods (i.e., Au{100} facets) are only partially covered by silver, and therefore grow faster, which leads to the one-dimensional growth along the [100] direction. The ratio of growth rates between Au{100} and Au{110} is adjustable by varying the Ag(I) concentration, which explains the fact that the aspect ratio is controlled by the Ag(I) concentration.

The formation of gold bipyramids can be explained in a similar way. The bipyramids are grown from gold seeds *II*, which leads to the penta-fold twinned gold nanorods in CTAB solution without Ag(I) added. For the nanorods, the growth rate along the twinning axis is faster than the one perpendicular to it (i.e., the growth of Au{100} facets) because of the selective adsorption of Br^- on Au{100}.[17] This relation still holds for the growth with Ag(I) since the concentration of Br^- and CTA^+ is the same. A quasi-one-dimensional nanostructure is therefore expected. However, as the nanostructure grows along the twinning axis, the Au{100} side walls cannot be always flat. Instead, steps should appear along the growth direction. These steps are not thermodynamically stable and finally disappear from the nanorods. The situation is different when Ag(I) is present in the growth solution. The steps provide open sites with a probably larger UPD shift for silver deposition. Therefore, the steps may be stabilized with the assistance of Ag(I), resulting in the unique shape of the bipyramid.

Conclusion

In summary, we systemically studied the Ag(I) assisted seed-mediated growth of gold anisotropic structures in CTAB solution. We reported that the initial twinned structures of the gold seeds are determinant for the final structures. Starting from seeds in the range of 2−3 nm, we found that one type of seed is primarily single crystalline and another is multiply twinned, some with an idealized shape of decahedron.

In the presence of Ag(I), the growth from the single crystalline seeds leads predominantly to single crystalline gold nanorods, with the growth direction as a [100] axis and the side faces as {110} and {100} facets. The growth from the twinned seeds gives in good yield elongated bipyramid nanoparticles with a very monodisperse shape. The structural characterization reveals that the bipyramids are penta-fold twinned around the growth axis, with the side {100} facets tilted toward the {111} facets. The observed angle suggests a highly stepped (11*n*) (*n* is ∼7) surface corresponding to one step every three or four atomic rows along the growth direction.

These novel structures present the sharpest longitudinal plasmon resonance around 1.5 eV yet reported. This is a significant improvement over rods for which the aspect ratio is not so well-constrained. The inhomogeneous width of the bipyramids can be as small as 0.13 eV for a homogeneous width of 0.095 eV. This uniquely monodispersed plasmon resonance arises from a tight control of the aspect ratio of the bipyramids, which is fully determined by the angle of the facets.

Finally, considering that both single crystalline nanorod and bipyramid nanostructures have high-energy surface structures, a new explanation is given for the essential role of Ag(I). It is the earlier underpotential deposition onset of Ag(I) on the more open (110) and steps that leads to an Ag(0) monolayer or submonolayer coverage. The modified surfaces therefore grow more slowly and become dominant in the final structures. This new role of Ag(0) as a surface structure specific surfactant provides a satisfactory explanation of the initially puzzling differences between the two gold nanorod preparation procedures that had been in the literature. The underpotential deposition of impurity metals may provide a general mechanism to control shape evolution in metallic nanostructures.

Acknowledgment. This work was supported by the University of Chicago MRSEC NSF-DMR under Grant DMR-0213745.

References and Notes

(1) Kreibig, U.; Vollmer, M. *Optical properties of metal clusters*; Springer: Berlin; New York, 1995.
(2) Bohren, C. F.; Huffman, D. R. *Absorption and scattering of light by small particles*; Wiley: New York, 1983.
(3) Duff, D. G.; Curtis, A. C.; Edwards, P. P.; Jefferson, D. A.; Johnson, B. F. G.; Kirkland, A. I.; Logan, D. E. *Angew. Chem., Int. Ed. Engl.* **1987**, *26*, 676−678.
(4) Jin, R. C.; Cao, Y. W.; Mirkin, C. A.; Kelly, K. L.; Schatz, G. C.; Zheng, J. G. *Science* **2001**, *294*, 1901−1903.
(5) Averitt, R. D.; Sarkar, D.; Halas, N. J. *Phys. Rev. Lett.* **1997**, *78*, 4217−4220.
(6) Sun, Y. G.; Xia, Y. N. *Science* **2002**, *298*, 2176−2179.
(7) Yu, Y. Y.; Chang, S. S.; Lee, C. L.; Wang, C. R. C. *J. Phys. Chem. B* **1997**, *101*, 6661−6664.
(8) Jana, N.; Gearheart, L.; Murphy, C. *J. Phys. Chem. B* **2001**, *105*, 4065−4067.
(9) Murphy, C.; Jana, N. *Adv. Mater.* **2002**, *14*, 80−82.
(10) Nikoobakht, B.; El-Sayed, M. A. *Chem. Mater.* **2003**, *15*, 1957−1962.
(11) Sun, Y. G.; Mayers, B.; Herricks, T.; Xia, Y. N. *Nano Lett.* **2003**, *3*, 955−960.
(12) Liu, M. Z.; Guyot-Sionnest, P. *J. Phys. Chem. B* **2004**, *108*, 5882−5888.

(13) Gersten, J.; Nitzan, A. *J. Chem. Phys.* **1980**, *73*, 3023−3037.
(14) Van der Zande, B. M. I.; Bohmer, M. R.; Fokkink, L. G. J.; Schonenberger, C. *J. Phys. Chem. B* **1997**, *101*, 852−854.
(15) Wang, Z.; Mohamed, M.; Link, S.; El-Sayed, M. *Surf. Sci.* **1999**, *440*, L809−L814.
(16) Wang, Z. L.; Gao, R. P.; Nikoobakht, B.; El-Sayed, M. A. *J. Phys. Chem. B* **2000**, *104*, 5417−5420.
(17) Johnson, C. J.; Dujardin, E.; Davis, S. A.; Murphy, C. J.; Mann, S. *J. Mater. Chem.* **2002**, *12*, 1765−1770.
(18) Perez-Juste, J.; Liz-Marzan, L. M.; Carnie, S.; Chan, D. Y. C.; Mulvaney, P. *Adv. Funct. Mater.* **2004**, *14*, 571−579.
(19) Chang, S. S.; Shih, C. W.; Chen, C. D.; Lai, W. C.; Wang, C. R. C. *Langmuir* **1999**, *15*, 701−709.
(20) Jana, N. R.; Gearheart, L.; Murphy, C. J. *Adv. Mater.* **2001**, *13*, 1389−1393.
(21) Jana, N. R.; Gearheart, L.; Obare, S. O.; Murphy, C. J. *Langmuir* **2002**, *18*, 922−927.
(22) Sau, T. K.; Murphy, C. J. *Langmuir* **2004**, *20*, 6414−6420.
(23) Gole, A.; Murphy, C. *Chem. Mater.* **2004**, *16*, 3633−3640.
(24) Duff, D.; Curtis, A.; Edwards, P.; Jefferson, D.; Johnson, B.; Logan, D. *J. Chem. Soc., Chem. Commun.* **1987**, 1264−1266.
(25) Curtis, A. C.; Duff, D. G.; Edwards, P. P.; Jefferson, D. A.; Johnson, B. F. G.; Kirkland, A. I.; Wallace, A. S. *J. Phys. Chem.* **1988**, *92*, 2270−2275.
(26) Zweifel, D. A.; Wei, A. *Chem. Mater.* **2005**, *17*, 4256−4261.
(27) Sonnichsen, C.; Franzl, T.; Wilk, T.; von Plessen, G.; Feldmann, J.; Wilson, O.; Mulvaney, P. *Phys. Rev. Lett.* **2002**, *88*, 077402.
(28) Lisiecki, I.; Filankembo, A.; Sack-Kongehl, H.; Weiss, K.; Pileni, M. P.; Urban, J. *Phys. Rev. B* **2000**, *61*, 4968−4974.
(29) Lisiecki, I. *J. Phys. Chem. B* **2005**, *109*, 12231−12244.
(30) Pal, T.; De, S.; Jana, N. R.; Pradhan, N.; Mandal, R.; Pal, A.; Beezer, A. E.; Mitchell, J. C. *Langmuir* **1998**, *14*, 4724−4730.
(31) Kolb, D. M. In *Advances in electrochemistry and electrochemical engineering*; Gerisher, H., Tobias, C. W., Eds.; Wiley: New York, 1978; Vol. 11.
(32) Herrero, E.; Buller, L. J.; Abruna, H. D. *Chem. Rev.* **2001**, *101*, 1897−1930.
(33) Kolb, D. M.; Przasnyski, M.; Gerischer, H. *J. Electroanal. Chem.* **1974**, *54*, 25−38.
(34) Rogers, L. B.; Krause, D. P.; Griess, J. C.; Ehrlinger, D. B. *J. Electrochem. Soc.* **1949**, *95*, 33−46.
(35) Leiva, E. *Electrochim. Acta* **1996**, *41*, 2185−2206.
(36) Ogaki, K.; Itaya, K. *Electrochim. Acta* **1995**, *40*, 1249−1257.
(37) Ikemiya, N.; Yamada, K.; Hara, S. *Surf. Sci.* **1996**, *348*, 253−260.
(38) Sanchez, C. G.; Del Popolo, M. G.; Leiva, E. P. M. *Surf. Sci.* **1999**, *421*, 59−72.
(39) Rojas, M. I.; Sanchez, C. G.; Del Popolo, M. G.; Leiva, E. P. M. *Surf. Sci.* **2000**, *453*, 225−228.
(40) Hamelin, A. *J. Electroanal. Chem.* **1984**, *165*, 167−180.
(41) Hamelin, A.; Lipkowski, J. *J. Electroanal. Chem.* **1984**, *171*, 317−330.